

Modal analysis of kagome-lattice structures

This content has been downloaded from IOPscience. Please scroll down to see the full text.

2015 Laser Phys. Lett. 12 055102

(<http://iopscience.iop.org/1612-202X/12/5/055102>)

View [the table of contents for this issue](#), or go to the [journal homepage](#) for more

Download details:

IP Address: 93.180.54.153

This content was downloaded on 05/01/2016 at 13:02

Please note that [terms and conditions apply](#).

Modal analysis of kagome-lattice structures

H Perez¹, S Blakley¹ and A M Zheltikov^{1,2,3}

¹ Department of Physics and Astronomy, Texas A&M University, College Station, TX 77843, USA

² Physics Department, International Laser Center, MV Lomonosov Moscow State University, Moscow 119992, Russia

³ Russian Quantum Center, ul Novaya 100, Skolkovo, Moscow Region 143025, Russia

E-mail: zheltikov@physics.msu.ru

Received 20 February 2015

Accepted for publication 25 February 2015

Published 13 April 2015



Abstract

The first few lowest order circularly symmetric electromagnetic eigenmodes of a full kagome lattice are compared to those of a kagome lattice with a hexagonal defect. This analysis offers important insights into the physics behind the waveguiding properties of hollow-core fibers with a kagome-lattice cladding.

Keywords: kagome cladding, hollow-core fiber, waveguide dispersion

(Some figures may appear in colour only in the online journal)

Hollow fibers with a kagome-lattice cladding are part of a class of broadband guiding fibers that are able to guide light through an inhibited coupling between core and cladding modes [1]. This type of fiber exhibits broad regions of low loss guidance interspersed with high loss regions corresponding to frequencies where cladding modes with slow azimuthal variation approach their cut-off and are then able to couple strongly to core modes as a result of diminished refractive index difference and an increased field overlap compared with modes of higher azimuthal dependence. Hollow fibers with a kagome cladding have been shown to enable efficient multioctave supercontinuum generation [2] and pulse compression to subcycle pulse widths and gigawatt peak powers [3]. Similar in structure to a kagome fiber, and a kind of precursor to this fiber in the manufacturing stage, is a lattice of tubes stacked in a triangular arrangement (triangular tube lattice, see figure 1(b)). Vincetti and Setti [4] used the finite-element method (FEM) to show that dispersion of core and cladding modes in a triangular tube lattice waveguide is accurately predicted by dispersion for a single dielectric tube, except at regions of high loss. Since a triangular tube lattice has much in common with a kagome lattice that has been perturbed, we expect similar relations to hold true for the modes

of a kagome lattice and dispersion of a single hexagonal tube. Additional support for this idea comes from references [5] and [6], which point to the antiresonance effects of the immediate core surround as the main influence on transmission in these types of fibers.

Previous authors have commented on the ability to tailor dispersion of microstructured fibers, including semi-periodically structured fibers, due to their sensitive dependence on geometry [7]. As a dramatic example, consider two microstructured fibers drawn from the same triangular tube lattice preform. Depending on how the hollow portions of the stack are pressurized during the drawing process, we can produce either a photonic band gap fiber [8–14] or a kagome [1, 15–17] fiber, the two of which guide light in fundamentally different ways [1, 18, 19]. Due to the highly geometric nature of the kagome lattice we expect to find some correlation between the geometric features in the kagome structure and its guidance characteristics.

In this work, we present a comparative modal analysis for a kagome lattice and a kagome lattice with a hexagonal defect (see figure 1(a)). Fully-vectorial eigenmodes of Maxwell's equations with periodic boundary conditions were computed by preconditioned conjugate-gradient

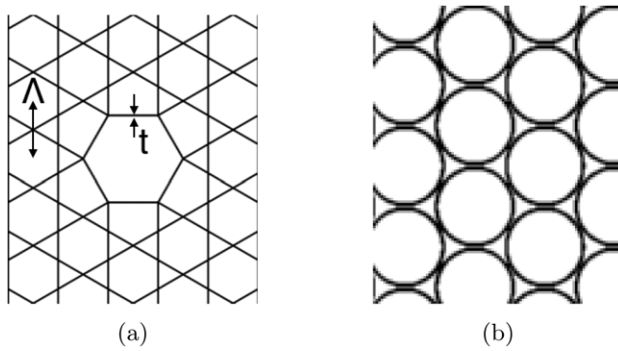


Figure 1. (a) Example section of a fiber cross-sectional geometry with a kagome-lattice cladding and central hexagonal defect. Indicated within are the pitch Λ and glass thickness t . (b) Section of a triangular tube lattice.

minimization of the block Rayleigh quotient in a planewave basis, using a freely available software package [20]. This software takes a propagation constant as input on a given dielectric structure and outputs definite-frequency modes. We used this software to study mainly the fundamental mode of the defect and a few lattice modes that we identified as being related to the defect modes. The computed modes were output in terms of a scale invariant normalized frequency $\alpha = \Lambda/\lambda$ where we have taken Λ to be the lattice pitch and λ is the free space wavelength. All the modeled geometries considered were given glass struts of index $n = 1.45$, corresponding to silica glass, and transverse thickness $t = 0.0346\Lambda$. Because we have used a flat material dispersion throughout the frequency range considered, this work has greatest potential for application in the frequency range between ultraviolet and mid-IR.

To map dispersion, we identified modes based on their transverse power profile. As expected, the lowest frequency mode observed within the defect possessed an approximately circularly symmetric profile, bearing similarity to the HE_{11} mode of a circular fiber. It is this mode which we call the fundamental mode. We also proceeded to map the dispersion for airy cladding modes bearing similarity to the fundamental defect mode, albeit in a kagome lattice without a defect. For the sake of comparison, we refer to these modes that appear within the hexagonal air holes as fundamental modes of the lattice. As we mapped the dispersion for the fundamental defect mode we noticed apparent discontinuities in the curve where the fundamental mode seemed to hop down in effective index as frequency increased. We expect the lossy regions mentioned earlier to overlap with these discontinuous or perturbed regions. However, we note that this type of simulation with periodic boundary conditions gives no information on the attenuation of a mode, so we were unable to confirm this. Upon inspection of the power profiles of some of the defect modes near the discontinuity it appeared that the fundamental mode for frequencies higher than the point of discontinuity evolved from a set of modes which were considered higher order modes at frequencies lower than the point of discontinuity. Combining this set

of modes shows that they most closely resembled the next order circularly symmetric mode of a circular fiber. As can be seen in figure 2, some of the modes found by our software in this range carry a brighter central spot which is approximately circularly symmetric. It is these higher order modes that we follow and plot below in addition to the fundamental mode. Mapping these higher order modes did in fact match up with the lowered dispersion curves and extended them to lower frequencies (see figure 3). The dispersion for the lattice modes was found to show the same behavior as for the corresponding defect modes (figure 4).

Reference [4] uses an approximate expression for the dispersion of modes in a cylindrical air hole within a dielectric of infinite extent and show that this expression accurately predicts dispersion in both a hexagonal defect in a triangular tube lattice waveguide and the airy cladding modes of the triangular tube lattice. We checked if the modes of a single hexagonal tube were good predictors for the dispersion of modes in a kagome lattice (figure 5) and also included the dispersion as approximated by a cylindrical dielectric waveguide as was done in [4] and given by: $n_{\text{eff}} = 1 - \frac{1}{2} \left(\frac{u_{mn}\Lambda}{2\pi R\alpha} \right)^2$. Where α is normalized frequency, u_{mn} is the n th zero of the m th Bessel function J_m , and R is the radius of the air core found by $R = \frac{1}{2}(R_1 + R_2)$ where R_1 is the apothem and R_2 is the circumradius of the hexagonal air hole. Using this same relation to predict dispersion in our modeled geometries shows that it is also reasonably accurate for fibers with a hexagonal defect in a kagome cladding, and we see in figure 5 that the modes for each structure mentioned agrees pretty well, as we initially expected. We would like to mention that the data acquired for the modes of a single hexagonal tube through our software may be slightly skewed due to the inherent assumption of a periodic tiling of our computational cell through all space. However, we have tried to mitigate this source of inaccuracy by using a large computational cell compared to the transverse size of the tube.

The similarities and differences between the lattice and defect led us to wonder if there was a more geometric approach to explaining regions of high loss. While taking a look at the full kagome lattice, we noticed that for a given kagome lattice—which we shall call the base lattice—kagome lattices of larger dimension can be overlaid on this base lattice (see figure 6). Considering our base lattice as if it were comprised of each of these separate overlaid structures occupying the same space, suggests that modes available to a kagome lattice at one scale may interfere with modes of the same frequency for an overlaid kagome lattice of different scale. Let Λ_0 be the pitch of the base structure. Then the pitch of an overlaid structure will be given by $\Lambda = m^*\Lambda_0$, with m an odd integer. Recall that the frequency of a mode is a normalized frequency given as lattice pitch over wavelength, so to compare the frequencies of the modes available to the overlaid structures to those of the base structure we simply scale the base frequencies by the size ratio of the two structures.

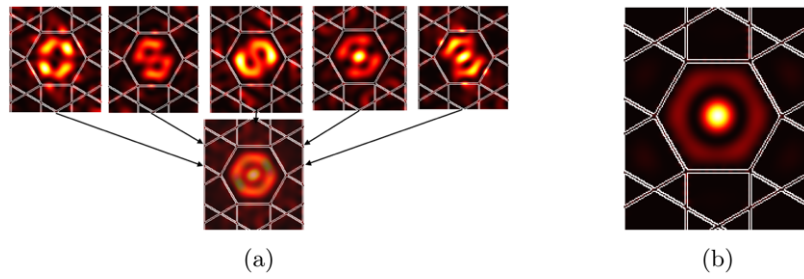


Figure 2. (a) Above is the spread of modes near to each other in frequency that are seen in a perturbed region. Below that are those five modes overlapped to show the circularly symmetric mode they are related to. (b) Farther from this region single modes more closely approximate the circularly symmetric modes.

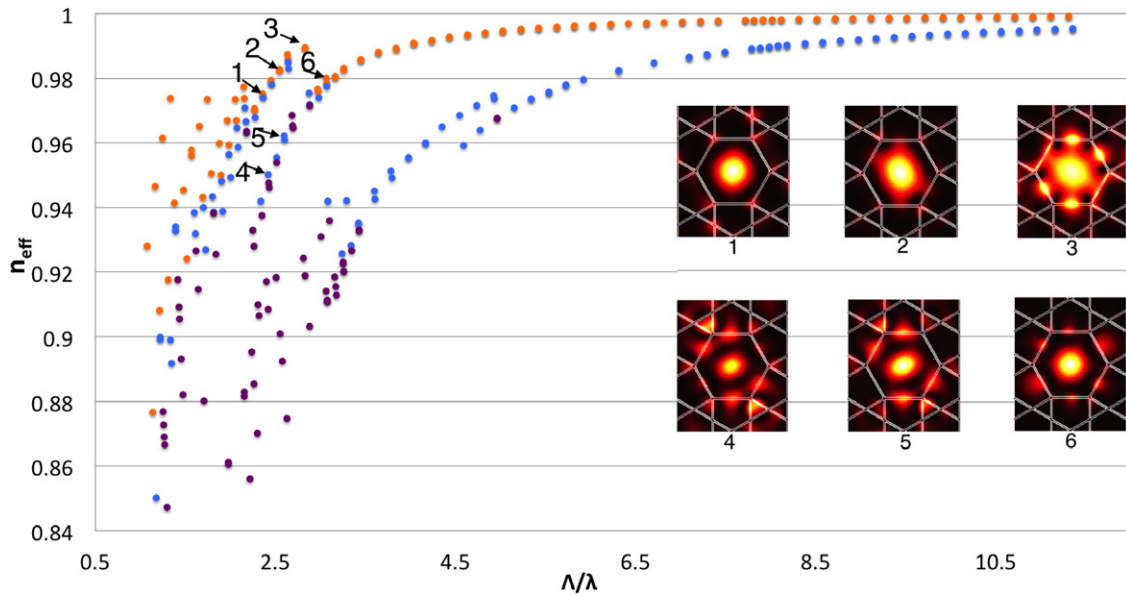


Figure 3. Effective index versus normalized frequency for the geometry seen in the insets. Top row of insets, numbered 1–3, show evolution of lower frequency fundamental mode as it approaches cutoff. Lower row of insets (4–6) show evolution of a higher order mode to new fundamental mode.

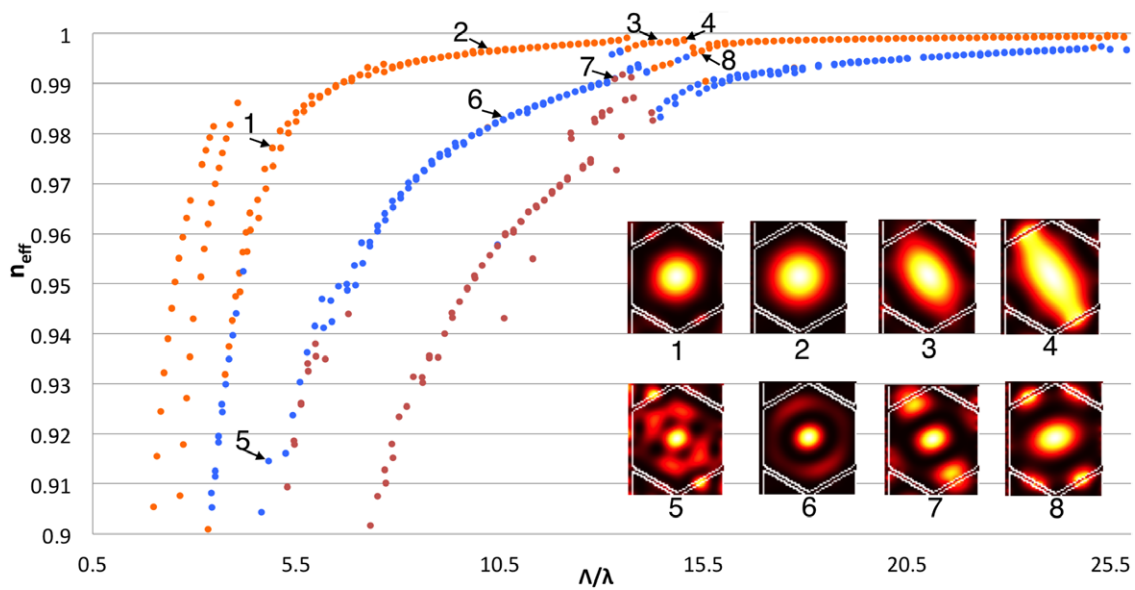


Figure 4. Effective index versus normalized frequency for the airy modes of the full kagome lattice. Top row of insets, numbered 1–4, show evolution of lower frequency fundamental mode as it approaches cutoff. Lower row of insets (5–8) show evolution of a higher order mode to new fundamental mode.

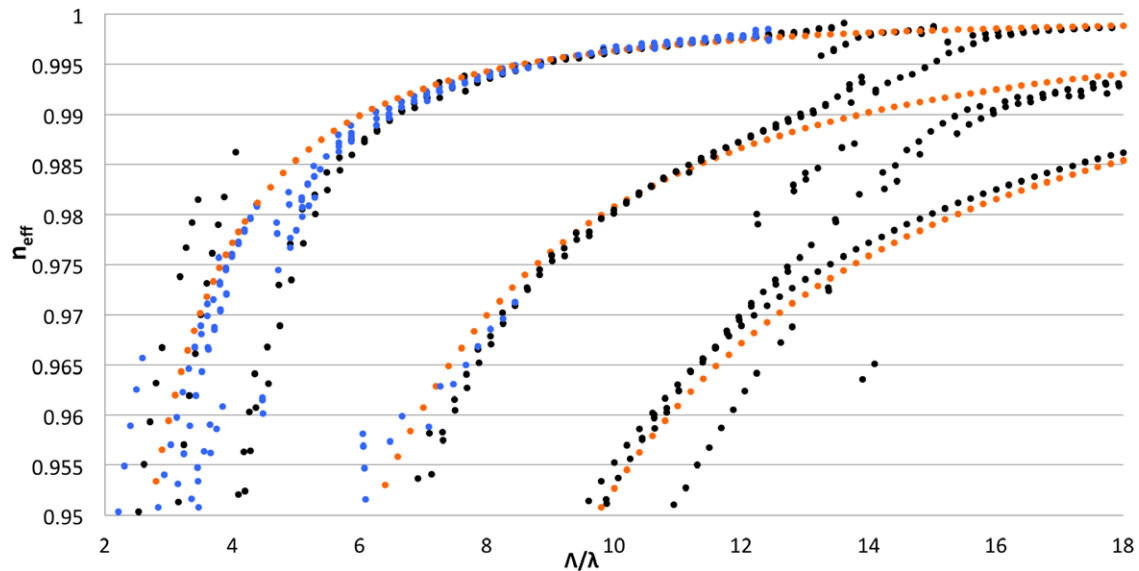


Figure 5. Dispersion of airy modes in kagome lattice (black), of a single hexagonal tube (blue), and using the approximation for a cylindrical dielectric waveguide (orange).

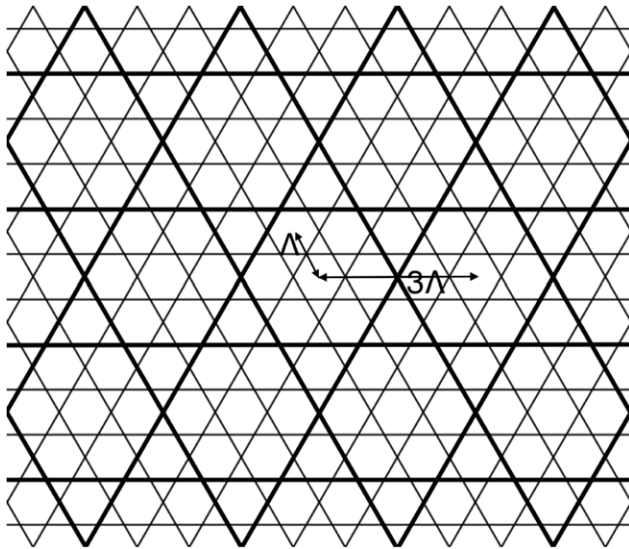


Figure 6. Kagome lattice with an example of a scaled overlaid kagome lattice shown in bold.

There is some subtlety though, in that our base lattice has a finite thickness, so the ratio of strut thickness to lattice spacing is not constant across the different scales. In the case of a real fiber, we believe that the smallest scale structure will be the most influential since it is the most abundant and larger structures will diminish in importance as their availability goes down.

We expected to find that the areas of perturbation for the base lattice dispersion curve coincided with crossings of scaled lattice dispersion curves. Instead we found that the scaled curves were shifted left in such a way that the curves for higher order circularly symmetric modes for a given structure more or less lay on top of the curves for lower order circularly symmetric modes of a smaller scale

structure, deviating much more around the inflection points (figure 7). What this suggests, is that the high density of modes for larger structures in the low frequency regions perturbs the modes of the base hexagon as they try to couple to these. This, coupled with the similar behavior observed in figures 3 and 4, led us to believe that scaling the lattice curves to the defect sizes may provide a more accurate representation of the defect curves.

The pitch Λ is twice the length of one side of a lattice hexagon, and so we take the length of the side of a hexagon as our length for comparison when looking at the defect modes. As we see in figure 8, the dispersion for the defect modes follows the scaled lattice curves very closely. We noticed that the dispersion curves for the defect hole modes lacked or had diminished perturbation compared to the lattice curve scaled to the defect dimensions, with the defect most resembling a structure from an overlaid lattice following the lattice behavior closest (compare figures 8–11). For defect modes, perhaps the limited amount of structural replicas or the mismatch in geometry allows for interference effects as seen in the lattice curves to be mitigated.

In conclusion, we have verified the importance of the core surround and demonstrated that defect mode dispersion curves can be predicted by scaling the lattice dispersion, which can be simulated at a much lower computational cost. The scaling we have introduced does at least as well as the cylindrical hole approximation, with the possibility of adding some predictive ability for the lossy regions. We have also shown that the cladding geometry has a significant influence on the guiding properties of kagome-cladding fibers. We believe that this insight will aid in the design of fibers with kagome or kagome-like cladding. For future work, motivated by the kagome lattices similarity to three different periodic dielectric structures which all exhibit band gaps, we hope to use simulation to study the

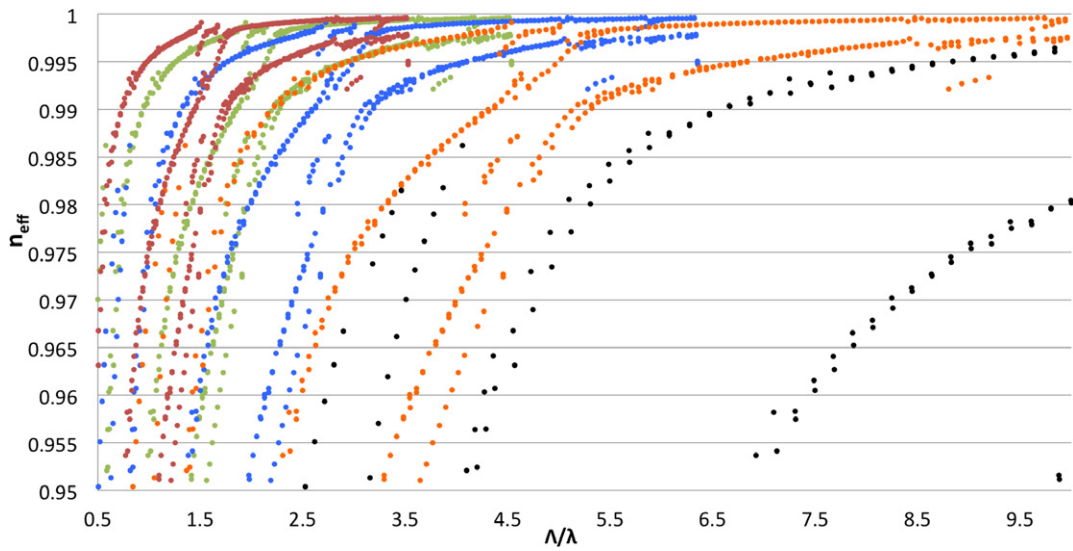


Figure 7. Lattice dispersion for fundamental mode (black curve) and the same curve scaled to the first few overlaid kagome lattices (orange for $3\lambda_0$, blue for $5\lambda_0$, green for $7\lambda_0$, and red for $9\lambda_0$).

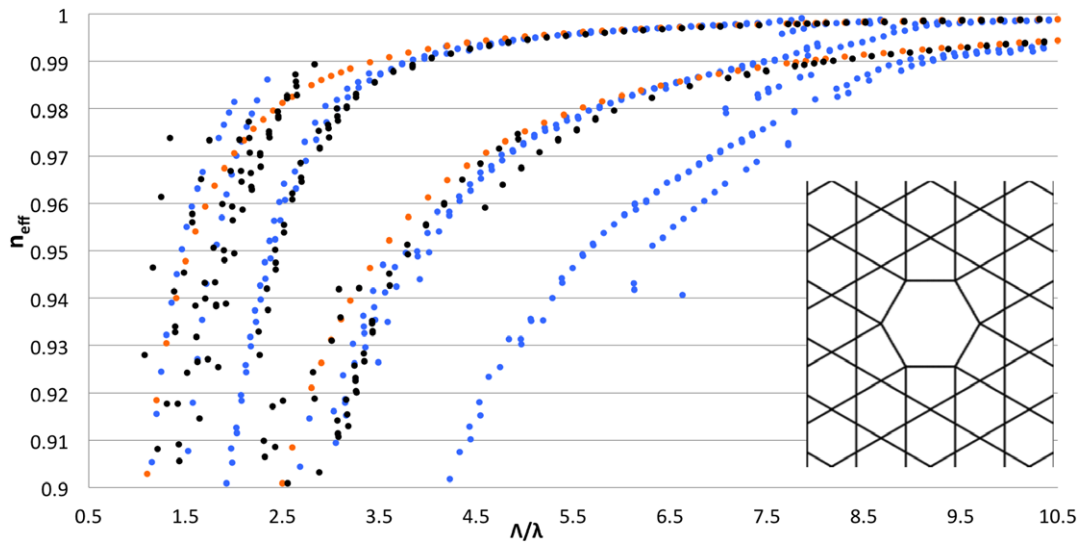


Figure 8. Dispersion for kagome lattice with the defect seen in the inset (black curve), lattice dispersion scaled by ratio of defect size to base hexagon size (blue curve), and cylindrical hole approximation (orange curve).

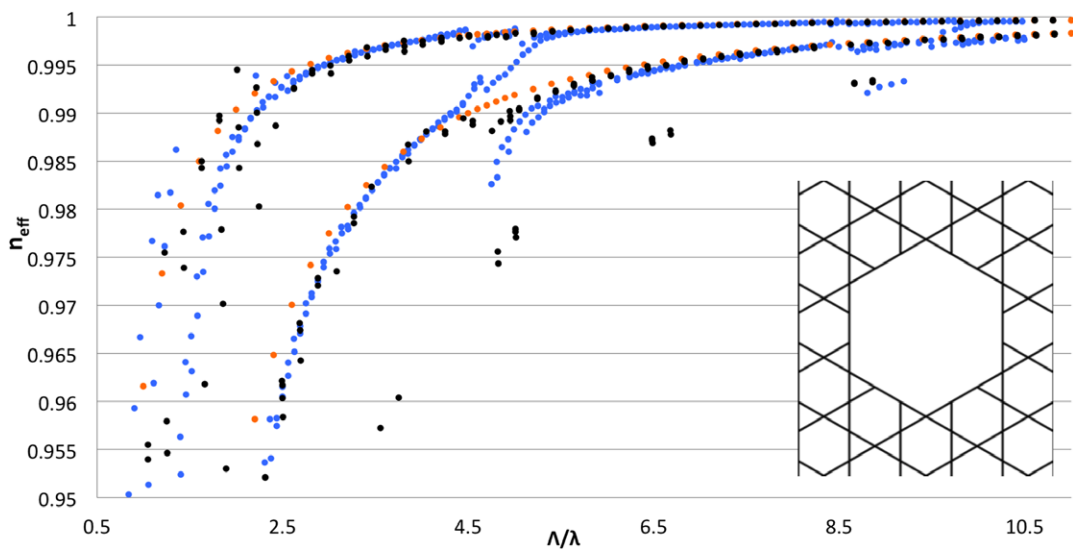


Figure 9. Dispersion of circularly symmetric modes for the geometry shown in the inset.

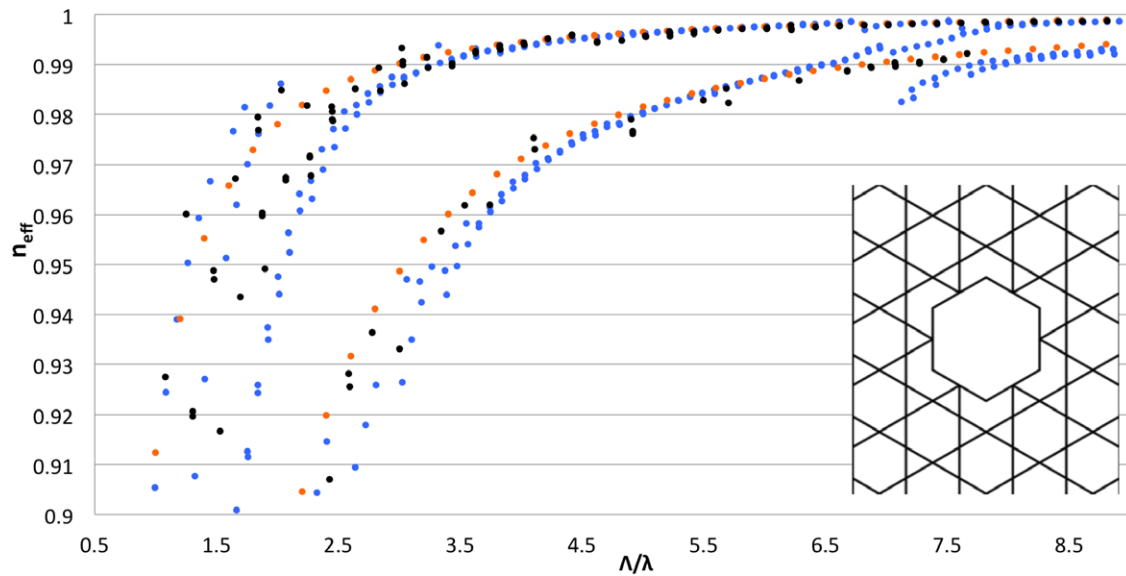


Figure 10. Dispersion of circularly symmetric modes for the geometry shown in the inset.

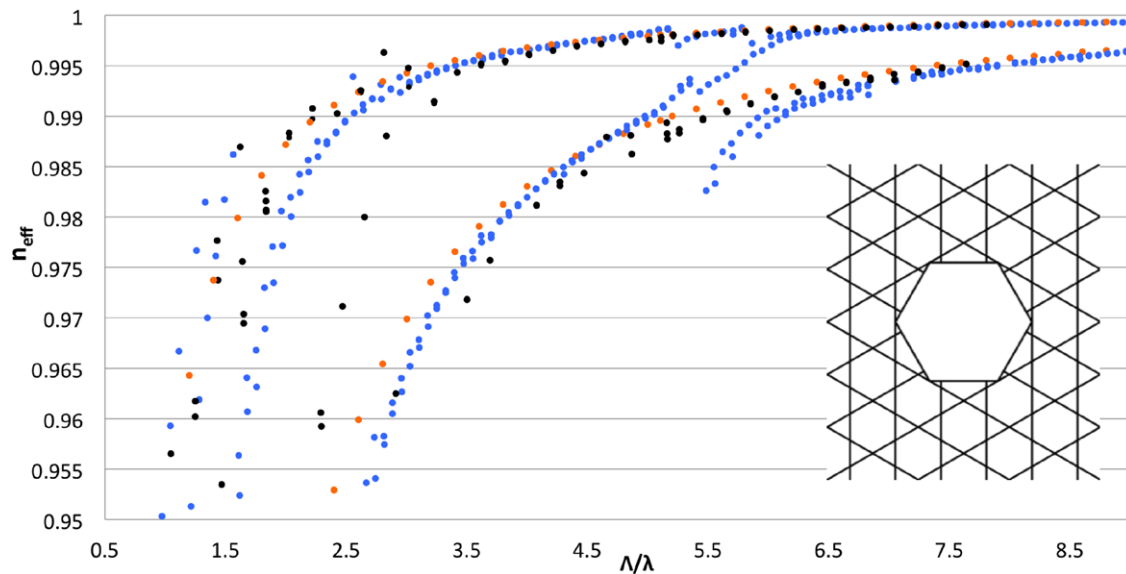


Figure 11. Dispersion of circularly symmetric modes for the geometry shown in the inset.

influence of band-gaps on the regions of guidance found in kagome fibers.

Acknowledgments

This research was supported in part by the Welch Foundation (Grant No. A-1801) and the Russian Foundation for Basic Research (project nos. 13-02-01465 and 14-29-07182). Research into waveguides for the mid-infrared range was supported by the Russian Science Foundation (project no. 14-12-00772).

References

- [1] Benabid F, Roberts P J, Couny F and Light P S 2009 *J. Eur. Opt. Soc.* **4** 09004
- [2] Couny F, Benabid F, Roberts P J, Light P S and Raymer M G 2007 *Science* **318** 1118–21
- [3] Balciunas T, Fourcade-Dutin C, Fan G, Witting T, Voronin A A, Zheltikov A M, Gerome F, Paulus G G, Baltuska A and Benabid F 2015 *Nat. Commun.* **6** 6117
- [4] Vincetti L and Setti V 2010 *Opt. Express* **18** 23133–46
- [5] Zheltikov A M 2008 *Phys.—Usp.* **51** 591–600
- [6] Fevrier S, Beaudou B and Viale P 2010 *Opt. Express* **18** 5142–50
- [7] Zheltikov A M 2004 *Phys.—Usp.* **47** 69–98
- [8] Cregan R F, Mangan B J, Knight J C, Birks T A, Russell P J, Roberts P J and Allan D A 1999 *Science* **285** 1537
- [9] Smith C M, Venkataraman N, Gallagher M T, Miller D, West J A, Borrelli N F, Allan D C and Koch K W 2003 *Nature* **424** 657
- [10] Zheltikov A M 2004 *Laser Phys. Lett.* **1** 220–33
- [11] Konorov S O, Mel'nikov L A, Ivanov A A, Alifimov M V, Shcherbakov A V and Zheltikov A M 2005 *Laser Phys. Lett.* **2** 366
- [12] Benabid F, Knight J C, Antonopoulos G and Russell P St J 2002 *Science* **298** 399–402

- [13] Russell P St J, Hölzer P, Chang W, Abdolvand A and Travers J C 2014 *Nat. Photon.* **8** 278–86
- [14] Konorov S O, Zheltikov A M, Zhou P, Tarasevitch A P and von der Linde D 2004 *Opt. Lett.* **29** 1521–3
- [15] Couny F, Benabid F and Light P S 2006 *Opt. Lett.* **31** 3574–6
- [16] Wang Y Y, Wheeler N V, Couny F, Roberts P J and Benabid F 2011 *Opt. Lett.* **36** 669–71
- [17] Wang Y Y, Light P S and Benabid F 2008 *IEEE Photon. Technol. Lett.* **20** 1018–20
- [18] Pearce G J, Wiederhecker G S, Poulton C G, Burger S and Russell P J 2007 *Opt. Express* **15** 12680–5
- [19] Zheltikov A M 2004 *Phys.-Uspekhi* **47** 1205–20
- [20] Johnson S G and Joannopoulos J D 2001 *Opt. Express* **8** 173–90